Theoretical Investigation of the Low- and High-Temperature MOVPE of Zinc Selenide

Carlo Cavallotti,* Davide Moscatelli, and Sergio Carrà

Department di Chimica, Materiali e Ingegneria Chimica "G. Natta", Politecnico di Milano, Via Mancinelli 7 − 20131 Milano, Italy

Received: August 4, 2003; In Final Form: November 14, 2003

The gas-phase chemistry active during the metal organic vapor-phase epitaxy of ZnSe from $Zn(CH_3)_2$ and H_2Se gas-phase precursors was studied theoretically with quantum chemistry. MP2 and QCISD(T) theories were used to investigate reactions that take place at low temperatures, when nonlocal forces were found to play an important role, whereas at high temperatures calculations were performed using density functional theory. Kinetic constants for each reaction were determined with conventional transition-state theory. It was found that the reactions of formation of the $H_2Se-Zn(CH_3)_2$, $[Zn(CH_3)_2]_2$, $[H_2Se]_2-Zn(CH_3)_2$, and $[Zn(CH_3)_2]_2-H_2Se$ clusters are exothermic by 4.6, 5.2, 9.9, and 12.5 kcal/mol, respectively. Equilibrium constants for the reactions of formation of the gas-phase clusters were determined using calculated energies and entropies. It was concluded that a significant amount of $Zn(CH_3)_2$ and H_2Se is present the gas phase as a cluster at room temperature. The reactivity of clusters was compared with that of dissociated $Zn(CH_3)_2$ and H_2Se, and it was found that reaction rates are enhanced because of the stabilization of transition states determined by increased electron donation to free d orbitals of Zn from Se molecules not directly taking part in the reaction process. The high-temperature process was found to differ substantially from the low-temperature one because of the presence of radicals generated at the growth surface, which can start a radical chain process that requires almost no activation energy. The validity of the gas-phase kinetic mechanisms here proposed was tested through a simulation of experimental reactors where the production of ZnSe gas-phase adducts was observed.

1. Introduction

Compound semiconductors are widely used in the production of solar cells, lasers, laser diodes, and light-emitting diodes (LED).[1] In particular, the process of metal organic vapor-phase epitaxy (MOVPE) of semiconductors suitable for optoelectronic applications in the field of blue-green light-emitting devices continues to receive much attention from the research community. This is due to the large demand for these compounds for new applications and the improvement of the current technologies that require the development of lasers, LEDs, and related detector working at short wavelengths (less than 600−550 nm). Materials that have these characteristics belong both to III-V and II-VI semiconductor compounds. The most promising materials in these fields are GaN and InP for the III-V compounds and ZnSe for II-VI. ZnSe compounds offer several advantages in comparison to III-V materials. First, the wide band gap of ZnSe makes it suitable for the manufacture of lasers emitting at 560 nm, which can be used as a light source for optical fibers produced with plastic material (PMMA).[2] Then, in the fabrication of conventional white LEDs, the use of ZnSe makes packaging less complicated and enlarges the overall efficiency of the device with respect to that of semiconductors containing phosphor. Moreover, the ZnSe substrate is conducting, allowing the use of top and bottom contacts, unlike GaN-on-sapphire devices, and is highly resistant to static electrical discharge because it operates at low voltage (2.7 V). Finally, ZnSe LEDs offer an extensive range of color temperatures (3500−8500 K).[3−5]

However, unlike the fast industrial commercialization of the MOVPE technology nowadays adopted to grow III-V compounds, the fabrication by MOVPE of II-VI heterostructures is hampered by the difficulties encountered in growing device-quality materials. A low growth temperature (<400 °C) and the absence of prereactions between II and IV precursors, along with reduced hydrogen incorporation during the growth process, are currently considered to be some of the major problems to be overcome.[5,6]

The identification of the key steps in the growth of ZnSe by MOVPE has been the subject of many theoretical and experimental investigations.[1] In fact, a knowledge of the growth kinetics would allow us to identify the reactions responsible for the formation of the defects present in the ZnSe films and would thus help us to improve the growth process. The MOVPE of ZnSe can be easily performed using H_2Se and $Zn(CH_3)_2$, obtaining a semiconductor with excellent electric and optical properties. Unfortunately, these precursors give severe prereactions in the gas phase, which are detrimental to the quality of the ZnSe film. To minimize the presence of defects in the growing film, we tested a number of different precursors. Alternative Zn-source precursors such as $Zn(C_2H_5)_2$ do not solve the problem of prereactions. Different Se-source precursors eliminate the prereactions but produce other problems. For example, precursors that are too stable, such as $(CH_3)_2Se$ and $(C_2H_5)_2Se$, cause an excessive decrease in the grow rate; CH_3-(allyl)Se causes heavy carbon contamination, and $(i\text{-}pr)_2Se$ and $(t\text{-}bu)_2Se$ are too stable for successful p doping.[1]

The MOVPE of ZnSe is usually conduced in a horizontal reactor where the deposition takes place on a wafer placed on a heated graphite susceptor. Growth temperatures and pressures are mostly included between 250 and 350 °C and between 20 and 250 Torr, respectively. At these operating conditions, gas-phase prereactions proceed very quickly. It is known that the

* To whom correspondence should be addressed. E-mail: carlo.cavallotti@polimi.it.

10.1021/jp036280x CCC: $27.50
Published on Web 01/22/2004

addition of the nitrogen donor adduct triethylamine (NET) contributes to eliminate the premature reaction between the reactants. The effect that NET has on the gas-phase reactivity and in particular on the suppression of gas-phase prereactions was studied in a recent theoretical study.[7] It was found that its effect is that of preventing the production of large gas-phase adducts through the formation of stable complexes with small ZnSe gas-phase molecules. Experimental studies have also shown that a significant amount of CH_4 is produced during the growth of the ZnSe film and that in the gas phase are present adducts of ZnSe such as CH_3ZnSeH and larger $CH_3(ZnSe)_xH$ oligomers. However, the exact nature of the gas-phase and surface reactions active during the growth process has not yet been established.[1,5]

Interestingly, it has recently been shown that it is possible to obtain the gas-phase nucleation of ZnSe nanoparticles that successively aggregate to form a ZnSe crystalline film at room temperature. These results were obtained through synthesis using a high concentration of precursors (H_2Se and $Zn(CH_3)_2$),[8] and ZnSe nanocrystals have been synthesized by microemulsion-gas contacting and in reverse micelles at similar temperatures. Experiments to produce nanocrystals were performed in a counterflow jet reactor in which ZnSe nanoparticles were formed by homogeneous nucleation near the stagnant point of the reactor. The aggregates consist of polycrystalline ZnSe nanoparticles with diameters of about 40 nm. The particles appear to be connected to each other by covalent bonds creating a fused "neck", typical for sintering. The particle is polycrystalline, consisting of single-crystalline grains with a characteristic size of about 4 nm and random orientation.[9] These results suggest that a kinetic pathway for the formation of large ZnSe adducts characterized by a small activation energy is active at low temperatures.

The aim of this work has been both to investigate the gas-phase kinetics responsible for the formation of gas-phase adducts during the high-temperature MOVPE of ZnSe and to determine the reactions that lead to the gas-phase nucleation of ZnSe observed at room temperature. Because of the large difference in temperature and gas-phase composition that characterizes the two growth processes, it is likely that two different kinetic pathways are active at high temperatures and low temperatures. We used two different approaches to investigate the gas-phase reactivity. Density functional theory was used when van der Waals forces were not playing a significant role. This was the case for reactions that occur at temperatures higher than 200 °C, such as those at which the ZnSe MOVPE is usually obtained. At room temperature, van der Waals forces can influence the gas-phase reactivity significantly. In this case, the intermolecular interactions were studied with the MP2 and QCISD theories. Conventional transition-state theory was then used to compute kinetic constants from calculated quantum chemistry data. The capability of the kinetic schemes so developed to reproduce experimental data was verified through the simulation of the performances of standard high- and low-temperature ZnSe growth reactors. Reactor simulations were performed with simple reactor models (i.e., CSTR and PFR), and their predictions should therefore be viewed as qualitative only.

2. Method

The gas-phase chemistry involving reactions for which van der Waals forces do not play a significant role was investigated with density functional theory. In particular, the Becke three-parameter and Lee−Yang−Parr hybrid functionals were used to evaluate the exchange and correlation energy.[10,11] This computational method has already given good results in the study of similar reacting systems.[12−14] Two different basis sets were used in the calculations: the all-electron 6-311G(d,p) basis set and a smaller one that adopts the Dunning−Huzinaga valence double-ξ basis set for the first-row atoms and the Stuttgart−Dresden effective core potential basis set for the others (briefly referred to as SDD in the following).[15,16]

TABLE 1: Comparison between Experimental and Calculated Bond Energies of Compounds Containing H, C, Zn, and Se Atoms[a]

bond energy	B3LYP SDD	B3LYP 6-311G(d,p)	QCISD 6-311G(d,p)	exptl
H−Se•	67.5	74.4	71.1	73.1 ± 0.5[35]
CH_3Zn-CH_3	64.8	65.2	69.6	68 ± 4[35]
Zn═Se	20.5	26.9	22.4	31.7 ± 3[36]
$CH_3Zn-SeH$	69.6	72.3	76.6	n.a.
H−H	104.7	104.0	102.7	104.2[35]
CH_3-H	103.2	102.5	101.7	102.5[35]

[a] Calculations were performed with DFT (B3LYP) and two different basis sets (SDD and 6-311G(d,p)) and the QCISD(T) theory with the 6-311G(d,p) basis set on geometries optimized at the MP2/6-311G(d,p) level. QCISD(T) energies were corrected with the higher-level correction approximation for correlation energy used in the G2MP2 method.[19] Data are reported in kcal/mol.

To evaluate the capability of DFT[17,18] to describe the Zn and Se gas-phase chemistry, available experimental bond energies of compounds containing Zn or Se atoms were compared with those calculated. The results are reported in Table 1, where bond energies calculated at the QCISD(T)/6-311G(d,p) level of theory are also reported for comparison. Here and in the following, bond energies were calculated as

$$\text{bond energy} = \sum_{\text{products}} (\text{EE} + \text{ThE}) - \sum_{\text{reactants}} (\text{EE} + \text{ThE}) \quad (1)$$

where EE is the correlated electronic energy of the system and ThE comprises the zero-point energy correction and the thermal energy (translational, rotational, and vibrational) required to heat the molecule from 0 to 298 K. For the QCISD(T) values, the higher-level correction of the correlation energy suggested in the G2MP2 method was added to the electronic energy of the system.[19] Good agreement with experimental data was obtained with the B3LYP/6-311G(d,p) theory. The following strategy was therefore used in the calculations: First, gas-phase structures of reactions of interest were computed with the SDD basis set. Then, the calculated geometries were used as input in the calculations with the larger basis set.

The kinetic mechanism active at low temperatures was investigated with the MP2[20] and the QCISD(T)[21] theories and the SDD basis set, which was preferred to the 6-311G(d,p) basis set for its smaller dimensions. In fact, under these conditions the van der Waals interactions between the molecules play an important role, and density functional theory cannot be used because of its inability to treat nonlocal forces.

Independently from the adopted level of theory, all geometries were optimized with the Berny algorithm and were considered stable only if they possessed no imaginary vibrational frequencies.[22] Vibrational frequencies smaller than 150 cm^{-1} were studied in detail and were considered to be rotors or hindered rotors when found necessary. In fact, small vibrational frequencies calculated in the harmonic oscillator approximation can be indicative of a small energetic barrier for the relative motion of a part of the molecule with respect to the other. Transition-state structures adopting the synchronous transit guided method were located and were characterized by a single imaginary vibrational frequency.[22] Kinetic constants were calculated with conventional

TABLE 2: Enthalpy Changes Calculated with Density Functional Theory (B3LYP) with Two Different Basis Sets (6-311G(d,p) and SDD) and Rate Coefficients Calculated with Transition-State Theory for the Direct Reactions and Expressed as $k = A \cdot \exp(-E_a/RT)$[a]

	reaction	ΔH 6-311G(d,p)	ΔH SDD	$\log_{10} A$	E_a
K_{dr1}	$Zn(CH_3)_2 + H_2Se \rightarrow TST_1$	−31.7	−34.2	8.75	19.6
K_{dr2}	$CH_3ZnSeH + Zn(CH_3)_2 \rightarrow TST_2$	−33.4	−35.6	7.57	19.4
K_{dr3}	$CH_3ZnSeH + H_2Se \rightarrow TST_3$	−28.7	−31.5	8.10	20.1

[a] Geometries, frequencies, and energies of the TS were calculated at the B3LYP/6-311G(d,p) level. The preexponential factor and activation energies are reported in units consistent with kcal, s, mol, and cm.

transition-state theory. All quantum chemistry calculations were performed with the Gaussian 98 suite of programs.[23]

3. Results and Discussion

3.1. Direct Reaction Mechanism. The reaction mechanism traditionally proposed in the literature to explain the formation of gas-phase ZnSe adducts involves the direct reaction between the precursors to give the CH_3ZnSeH molecule and CH_4.[1] In fact, in the metal organic precursors the bond energy between the metallic and the organic part of the molecule is too high to give homolytic bond fission in the temperature ranges at which the ZnSe MOVPE is usually conduced. After the formation of CH_3ZnSeH, it is generally assumed that the production of larger ZnSe adducts proceeds through a set of reactions in which Zn and Se units are successively added.[1] Here we investigated the first steps of this reaction mechanism, which are represented by the following reactions:

$$(CH_3)_2Zn + H_2Se \rightarrow CH_3ZnSeH + CH_4 \quad (2)$$

$$CH_3ZnSeH + (CH_3)_2Zn \rightarrow CH_3ZnSeZnCH_3 + CH_4 \quad (3)$$

$$CH_3ZnSeH + H_2Se \rightarrow HSeZnSeH + CH_4 \quad (4)$$

For each reaction, the enthalpy changes, reported in Table 2, were determined at the B3LYP level using both 6-311G(d,p) and SDD basis sets. All reactions are exothermic by about 30 kcal/mol. Kinetic constants were evaluated with conventional transition-state theory, and calculated preexponential factors and activation energies are reported in Table 2. It can be observed that activation energies of the three reactions investigated, computed at the B3LYP/6-311G(d,p) level, were found to be similar in all cases: 19.6, 19.4 and 20.1 kcal/mol, respectively. Accordingly, it is reasonable to assume that the formation of adducts of larger dimension such as $CH_3ZnSeZnSeH$ or HSeZnSeZnSeH would require overcoming a similar energetic barrier. Using the computed kinetic constant, the residence time in a perfect stirred reactor necessary to obtain a significant formation of the first ZnSe adduct in the gas phase can be easily determined as

$$\tau = \frac{C^{out}_{CH_3ZnSeH}}{K_R \cdot C^{in}_{Zn(CH_3)_2} \cdot C^{in}_{H_2Se}} = \frac{R \cdot T}{P} \cdot \frac{X^{out}_{CH_3ZnSeH}}{K_R \cdot X^{in}_{Zn(CH_3)_2} \cdot X^{in}_{H_2Se}} \quad (5)$$

where K_R is the kinetic constant of reaction 2, T and P are the temperature and the pressure, R is the gas constant, C_i represents the concentration in mol/L of the i^{th} chemical species, and X_i is its mole fraction. Typical operating conditions of reactors adopted to deposit ZnSe film are 250 Torr, 250 °C, and inlet mole fractions of precursors of about 10^{-3}.[1] Under such conditions, the residence time necessary to obtain the formation of a significant number of gas-phase adducts (i.e., 10^{-6}) is 2500 s. This time is much higher than the residence time in the reactor (about 10 s), which suggests that the rate at which the reaction between the precursors proceeds is too small to justify the formation of adducts. The same consideration also holds true for the low-temperature process because of the exponential decrease of the reaction kinetic constant.

To test the accuracy of the computed kinetic constants, we determined the activation energy of reaction 2 at a higher level of theory. For each chemical species, the value of the energy was calculated at the QCISD/6-311+G(d,p) level on geometries determined at the B3LYP/6-311G(d,p) level. The energies were then corrected for the basis set error using an approach similar to G2MP2[19] theory as

$$E(\text{MP2 correction}) = E(\text{MP2/6-311+G(3df,2p)}) - E(\text{MP2/6-311+G(d,p)}) \quad (6)$$

The activation energy so calculated is 17.25 kcal/mol, thus about 2.3 kcal/mol smaller than that determined at the B3LYP/6-311G(d,p) level. Because the correction is not large enough to significantly modify the residence time necessary to convert a significant number of precursors, it can be concluded that a reaction pathway different from those usually proposed to explain the formation of gas-phase adducts is probably active during the ZnSe MOVPE.

3.2. Low-Temperature Pathway: Homogeneous Nucleation. The kinetic pathways active at low temperatures are usually different from those determining the evolution of the reacting system at high temperatures. This is caused by the fact that under these conditions reactive species, such as radicals, that can be present at higher temperatures are not present. Moreover, at low temperatures intermolecular bonds of low energy are sufficient to bind two molecules together, thus determining the formation of clusters consisting of several molecules whose reactivity can differ even significantly from that of each molecule alone. Another reason for which the low-temperature reactivity of gas-phase molecules differs substantially from that at high temperature is that quantum effects, and in particular quantum tunneling, can significantly enhance the overall reaction rate.[24] This is particularly true for reactions characterized by the migration of a hydrogen atom from one molecule to another, which is the case for the reactions studied here.

$Zn(CH_3)_2$−H_2Se Gas-Phase Cluster Formation. To determine whether clusters containing $Zn(CH_3)_2$ and H_2Se molecules can be formed at room temperature, we investigated the following reactions that describe the first steps in the formation of gas-phase clusters:

$$H_2Se + Zn(CH_3)_2 \leftrightarrow H_2Se{-}Zn(CH_3)_2 \quad (7)$$

$$H_2Se{-}Zn(CH_3)_2 + H_2Se \leftrightarrow [H_2Se]_2{-}Zn(CH_3)_2 \quad (8)$$

$$H_2Se{-}Zn(CH_3)_2 + Zn(CH_3)_2 \leftrightarrow [Zn(CH_3)_2]_2{-}H_2Se \quad (9)$$

The amount of adducts formed through reaction 7−9 as a function of temperature is determined by the equilibrium

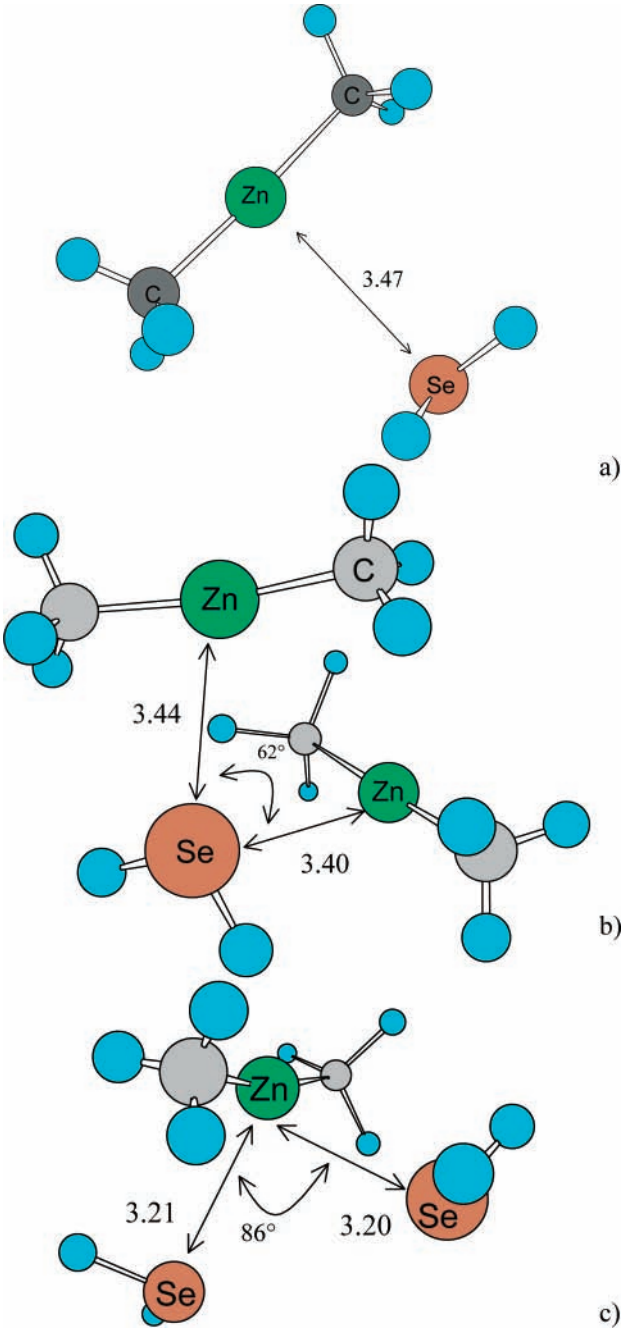

Figure 1. Optimized cluster structures for (a) $H_2Se-Zn(CH_3)_2$, (b) $[Zn(CH_3)_2]_2-H_2Se$, and (c) $[H_2Se]_2-Zn(CH_3)_2$. Geometries were calculated at the MP2/SDD level. Distances are reported in angstroms and angles in degrees.

constant K_{eq} of each reaction expressed as

$$K_{eq} = \exp\left(-\frac{\Delta G(T)}{RT}\right) = \prod x_i^{\nu i} \tag{10}$$

The higher K_{eq}, the larger the amount of clusters. The free-energy change is a function of the reaction enthalpy and entropy as $\Delta G(T) = \Delta H - T\Delta S$, where ΔH and ΔS are the enthalpy and entropy changes of the reaction, respectively. To calculate K_{eq}, we evaluated the enthalpy change of each reaction determining the energies at the QCISD(T)/SDD level on structures optimized at the MP2/SDD level. Calculated optimized structures and reaction enthalpy changes of reactions 7−9 and of other similar reactions are reported in Figure 1 and Table 3, respectively. The evaluation of the entropy of each Zn−Se cluster is a task complicated by the presence of several internal motions that cannot be treated as vibrational frequencies. To investigate this aspect, we calculated vibrational frequencies for each structure we optimized. Whereas structures were considered to be stable only if there were no negative vibrational frequencies, many small vibrational frequencies (i.e., lower than 150 cm^{-1}) were found. Such vibrational frequencies are indicative of the presence of internal molecular motions, such as torsional vibrations that have degenerated in free rotors or bending motions that have become 2D free rotors. The presence of many small vibrational frequencies is determined by the small strength of the van der Waals bond between the Zn and Se gas-phase molecules, which is not sufficient to block the relative positions of the molecules that are part of the cluster. The treatment of an internal motion as a vibration or as a rotation has a large impact on the calculation of the entropy of the gas-phase molecule. For this reason, we explicitly considered each small internal vibrational frequency with the aim of evaluating whether it should be treated as a rotor or as a vibration. The results of this study are summarized in Table 4. Using the values reported in Table 4, we evaluated the entropic contributions S_{int} of the internal rotations as

TABLE 3: Enthalpy Changes Calculated for Reactions Leading to the Formation of Gas-Phase Clusters[a]

reaction	ΔH (kcal/mol) QCISD(T)/SDD
$H_2Se + Zn(CH_3)_2 \rightarrow H_2Se-Zn(CH_3)_2$	−4.6
$2Zn(CH_3)_2 \rightarrow [Zn(CH_3)_2]_2$	−5.2
$H_2Se-Zn(CH_3)_2 + H_2Se \rightarrow [H_2Se]_2-Zn(CH_3)_2$	−5.3
$H_2Se-Zn(CH_3)_2 + Zn(CH_3)_2 \rightarrow [Zn(CH_3)_2]_2-H_2Se$	−7.9
$[Zn(CH_3)_2]_2 + H_2Se \rightarrow [Zn(CH_3)_2]_2-H_2Se$	−7.3

[a] Structures were optimized at the MP2/SDD level, and energies were calculated at the QCISD(T)/SDD level.

$$S_{int} = k_B \ln Q_{int} + k_B T\left(\frac{\partial \ln(Q_{int})}{\partial T}\right)_V \tag{11}$$

where Q_{int} is the partition function corresponding to the internal rotor, which is related to the moment of inertia I of the 1D or 2D internal rotation[25] as

$$Q_{rot}^{1D} = \frac{\pi^{1/2}}{\sigma} \cdot \left(\frac{k_B T}{B}\right)^{1/2} \tag{12}$$

$$Q_{rot}^{2D} = \left(\frac{k_B T}{B}\right) \tag{13}$$

B is equal to $h^2/8\pi^2 I$, k_B and h are the Boltzmann and Planck constants, respectively, and σ is the rotational symmetry number. The desired entropic contributions can thus be calculated as

$$S^{1D} = k_B\left(\ln \frac{1}{\sigma}\left(\frac{\pi k_B T}{B}\right)^{1/2} + \frac{1}{2}\right) \tag{14}$$

$$S^{2D} = k_B\left(\ln \frac{k_B T}{\sigma B} + 1\right) \tag{15}$$

Using the above-reported equations, we could then compute the correct entropy of each cluster. The calculated values were 70.6, 52.4, 118.2, 129.4, 162.9, and 146.0 cal/molK for $Zn(CH_3)_2$, H_2Se, $H_2Se-Zn(CH_3)_2$, $[Zn(CH_3)_2]_2$, $[Zn(CH_3)_2]_2-H_2Se$, and $[H_2Se]_2-Zn(CH_3)_2$, respectively.

Because of the small bond energies and the large entropies of the clusters, it is likely that the reactions that determine their

TABLE 4: Treatment of Internal Motions for Some Gas-Phase Molecules and Clusters[a]

	internal motions	ν cm^{-1}	B cm^{-1}	S cal/mol K
$Zn(CH_3)_2$	free relative rotation of the 2 CH_3 groups	21.	8.13	4.5
$H_2Se-Zn(CH_3)_2$	rotation of the CH_3 group of $Zn(CH_3)_2$	68.	8.13	4.5
	rotation of H_2Se with respect to $Zn(CH_3)_2$	9.0	6.7	5.5
	2D rocking motions of $Zn(CH_3)_2$ around the Zn−Se bond	47, 69	0.14	16.6
	2D rocking motions of H_2Se	119, 182	7.9	8.5
$[Zn(CH_3)_2]_2$	rotation of CH_3 of the first $Zn(CH_3)_2$ around the Zn−C axis	71.8	8.13	4.5
	rotation of CH_3 of the second $Zn(CH_3)_2$ around the Zn−C axis	75.0	8.13	4.5
	relative rotation of the two molecules on the Zn−C−Zn−C plane around the Zn−C axis	13.1	0.2	9.1
	rotation of the two molecules around the axis passing from C and perpendicular to the Zn−C−Zn−C plane	61.1	0.07	8.1
$[Zn(CH_3)_2]_2-H_2Se$	rotation of CH_3 in the first $Zn(CH_3)_2$	71.4	8.13	4.5
	rotation of CH_3 of the second $Zn(CH_3)_2$	86.1	8.13	4.5
	rotation of the first $Zn(CH_3)_2$	23.0	0.07	8.4
	rotation of the second $Zn(CH_3)_2$	63.7	0.07	8.4
	2D rocking motion of H_2Se	158, 174	7.7	8.5
$[H_2Se]_2-Zn(CH_3)_2$	rotation of CH_3 in $Zn(CH_3)_2$	68	8.13	4.5
	rotation of H_2Se with respect to $Zn(CH_3)_2H_2Se$	19.6	3.9	6.1
	2D rocking motion of the $Zn(CH_3)_2-H_2Se$ group	38.4, 42.2	7.6	20.5
	2D rocking motion of H_2Se	179, 154	1.0	8.5

[a] Vibrational frequencies were calculated at the MP2/SDD level. Moments of inertia for the internal rotations (reported as $B = h^2/8\pi^2 I$) were evaluated as suggested by Gilbert,[25] and entropies, as reported in the text.

TABLE 5: Calculated TST Rate Coefficients for the Reactions of Decomposition of the Gas-Phase Clusters to Give a ZnSe Adduct[a]

	reaction	$\log_{10} A$	E_a
K_{aut1}	$H_2Se-Zn(CH_3)_2 \rightarrow CH_3ZnSeH + CH_4$	11.5	24.1
K_{aut2}	$[H_2Se]_2-Zn(CH_3)_2 \rightarrow CH_3ZnSeH + CH_4 + H_2Se$	12.3	18.9
K_{aut3}	$[Zn(CH_3)_2]_2-H_2Se \rightarrow CH_3ZnSeH + CH_4 + Zn(CH_3)_2$	12.25	18.8

[a] Geometries were optimized at the MP2/SDD level, and energies were calculated with the QCISD(T) theory. Kinetic constants are expressed as $k = A \cdot \exp(-E_a/RT)$ and reported in units consistent with kcal, mol, cm, and s.

formation and dissociation proceed very quickly and can therefore be considered at equilibrium. This was confirmed by some preliminary calculations that we made evaluating kinetic constants with collisional theory and quantum chemistry, as explained in Cavallotti et al.[26] Using the calculated entropies and the reaction enthalpy values reported in Table 3, we calculated values of 211, 0.03, and 1.3 for the equilibrium constants of reactions 7, 8, and 9, respectively, at 298 K and 1 atm. Because equilibrium constants for reactions 7 and 9 are larger than unity, it is reasonable that at 298 K a consistent fraction of $Zn(CH_3)_2$ and H_2Se molecules will be present in the gas phase as clusters.

Reactivity of $Zn(CH_3)_2-H_2Se$ Gas-Phase Clusters. Clusters of $Zn(CH_3)_2$ and H_2Se molecules have a reactivity that can differ even significantly from that of the isolated molecules. Gas-phase clusters can lead to the formation of ZnSe adducts through the following set of reactions:

$$H_2Se-Zn(CH_3)_2 \rightarrow CH_3ZnSeH + CH_4 \quad (16)$$

$$[H_2Se]_2-Zn(CH_3)_2 \rightarrow CH_3ZnSeH + CH_4 + H_2Se \quad (17)$$

$$[Zn(CH_3)_2]_2-H_2Se \rightarrow CH_3ZnSeH + CH_4 + Zn(CH_3)_2 \quad (18)$$

The enthalpy change of each reaction was computed at the QCISD(T)/SDD level using geometries optimized at the MP2/SDD level. As expected, it was found that these reactions are exothermic by 30.68, 30.19, and 28.09 kcal/mol, respectively. Successive transition states for each reaction were determined at the same level of theory. Kinetic constants were calculated using conventional transition-state theory and are reported in Table 5, and transition-state structures are reported in Figure 2. It is interesting to observe that the 24.1 kcal/mol of activation energy calculated for the decomposition of the $H_2Se-Zn(CH_3)_2$ adduct can be compared with the 19.6 kcal/mol calculated for reaction 7 between the dissociated H_2Se and $Zn(CH_3)_2$ molecules because the 4.5 kcal/mol difference can be ascribed to the enthalpy of formation of the cluster, which decreases the bottom of the potential energy well by 4.6 kcal/mol, as reported in Table 3. This internal consistency of the calculations is important because the activation energy for reactions 7 and 16 was calculated using two different computational approaches (i.e., DFT and QCISD(T)). It is also important to observe that the activation energy for cluster dissociation reactions 17 and 18 is smaller by 5.3 kcal/mol than that calculated for reaction 16. This can be attributed to an effect of the stabilization of the transition state determined by the increase in the energy of the bond between the H_2Se or $Zn(CH_3)_2$ molecule of the cluster not directly taking part in the reaction and the Zn and Se reacting molecules. The stabilization effect can be ascribed to the increased electron donation from Se to the free d orbitals of

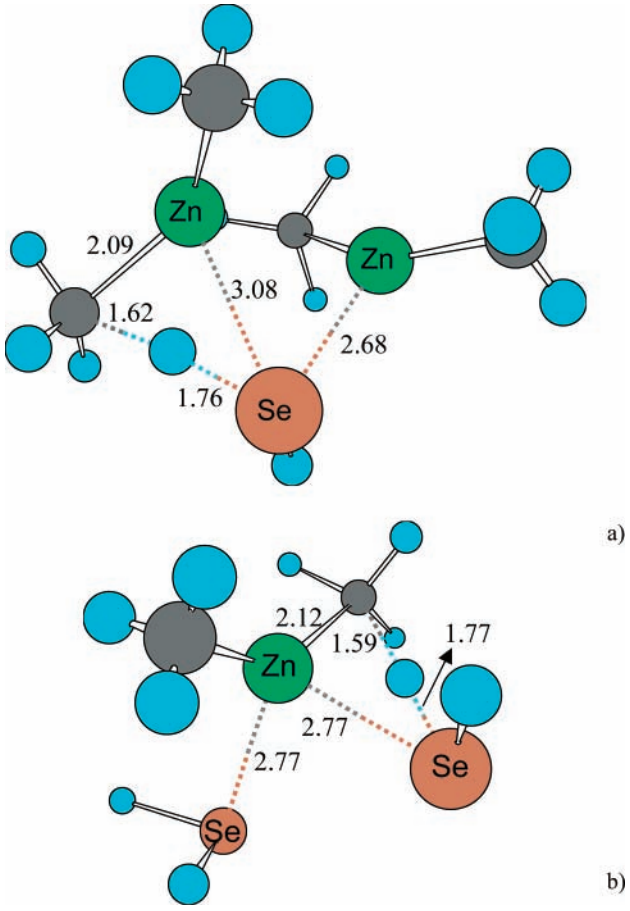

Figure 2. Transition-state structures for the reactions of the decomposition of the considered clusters: (a) $[Zn(CH_3)_2]_2-H_2Se \rightarrow TST_1$ and (b) $[H_2Se]_2-Zn(CH_3)_2 \rightarrow TST_2$. Geometries were calculated at the MP2/SDD level; distances are reported in angstroms.

Zn, which become more accessible as the $Zn-CH_3$ is being broken. In fact, the Zn−Se bond lengths between reacting and nonreacting groups of the cluster decrease from 3.4 and 3.2 Å for the relaxed cluster to 2.7 and 2.8 Å for the transition state.

To determine if the proposed mechanism can explain the gas-phase nucleation of ZnSe that was experimentally observed, we performed some simulations introducing the calculated kinetic constants in a PFR reactor model that could reproduce the experimental setup used by Mountziaris et al. to nucleate ZnSe in the gas phase.[8] The adopted kinetic mechanism comprises the reactions reported in Table 5 and assumes that the concentration of clusters, represented by reactions 7, 8, and 9, is at equilibrium, which is reasonable considering the relatively small bond energies of the clusters. The simulation has been performed at 25 °C and 125 Torr, adopting H_2 as the carrier gas. The precursors inlet mole fraction that was used was 0.02, and the total flow rate was 60 sccm. Simulations show that a significant amount of CH_3ZnSeH is produced as a result of the pathway proceeding through the cluster formation. A simulation under the same operating conditions adopted for this autocatalytic mechanism was performed using the direct reaction pathway. A comparison between the CH_3ZnSeH mole fraction produced, including the reactions involving the formation of clusters and that calculated considering only the direct reaction between $Zn(CH_3)_2$ and H_2Se, is shown in Figure 3. As can be observed, the maximum mole fraction of CH_3ZnSeH produced is 10^{-4} for the pathway involving the formation of gas-phase clusters and 5×10^{-11} when the formation of clusters was neglected.

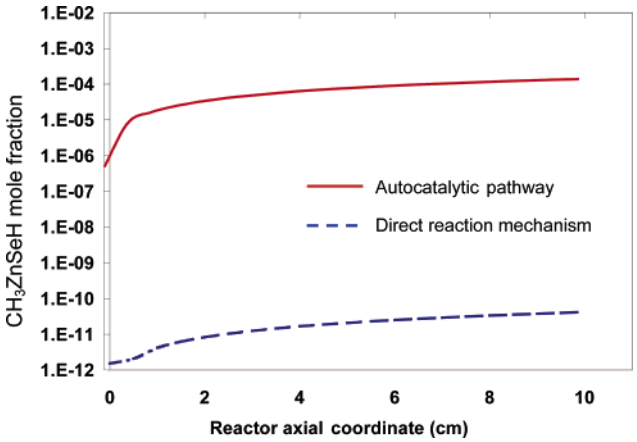

Figure 3. Comparison between the CH_3ZnSeH mole fraction produced through the autocatalytic pathway that requires the formation of intermediate gas-phase clusters and the direct reaction from the precursors. Simulations were performed at 25 °C and 125 Torr.

Although here we examined only the reaction pathways leading to the formation of the first ZnSe adduct, namely, CH_3-ZnSeH, it is likely that a similar set of reactions with similar kinetic constants are responsible for the successive growth of CH_3ZnSeH to give larger gas-phase adducts. It would therefore seem that the growth process proceeds through the successive formation of ZnSe adducts of increasing dimension until, once a critical dimension is reached, they coalesce to give the formation of nanoparticles.

Quantum Tunneling. Because the reaction between $Zn(CH_3)_2$ and H_2Se involves the migration of a hydrogen atom from Se to $Zn(CH_3)_2$ to form CH_4, it is possible, because of the small mass of H, that a quantum tunneling effect can be significant. It is in fact known that tunneling can enhance the kinetic constant values for reactions involving the transfer of a hydrogen atom by a factor depending on the value of the imaginary vibrational frequency of the transition state and on the temperature.[24] Though some equations have been proposed for the direct evaluation of the tunneling correction, of which the most used is the Wigner approximation,[27] it has been shown that especially at low temperatures these approximations can significantly underestimate the tunneling effect.[28] The use of higher-level theories for the calculation of the tunneling correction requires a knowledge of some details of the potential energy surface of the system. In particular, to apply the small curvature approximation method, it is necessary to know energy, gradient, and Hessian information along the reaction pathway.[24] The definition of the minimum-energy pathway for the reaction between $Zn(CH_3)_2$ and H_2Se to give CH_3ZnSeH and CH_4, which is the prototype of the reactions investigated here, is a task complicated by the fact that during the migration of H from H_2Se to CH_3 there is the concomitant formation of the Zn−Se bond and the cleavage of the $Zn-CH_3$ bond, which makes it difficult to define a reaction coordinate univocally. To solve this problem, we defined the 0 of the reaction coordinate s at the transition state; positive values of s represent the H−Se distance after the bond has been broken, and negative values represent the H−C distance as H is approaching C. The aim of this definition is to describe correctly the path along which H is moving while it is traveling from Se to C. The coordinates of all of the other atoms along the reaction pathway have been determined through molecular dynamics using quantum chemistry calculated forces assuming that each atom is at rest in the transition state and is moving toward reactants or products depending on the sign of the reaction coordinate. The calculated

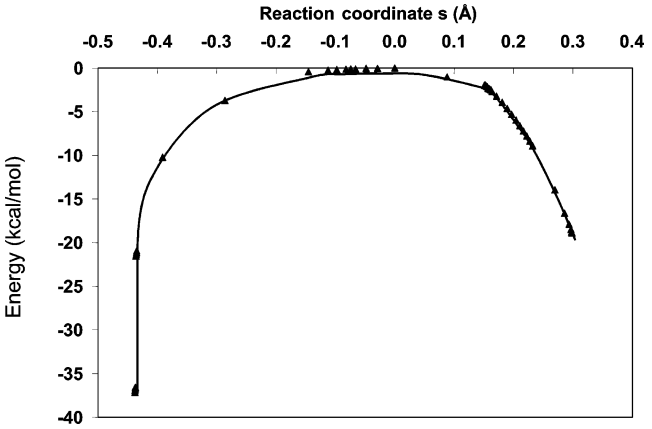

Figure 4. Plot of the potential energy along the reaction coordinate for the reaction between H_2Se and $Zn(CH_3)_2$. The reaction coordinate was defined so that its 0 is the transition state, positive values represent the H−Se distance after the bond has been broken, and negative values are the H−C distance as H is approaching C.

potential energy surface is reported in Figure 4. As can be observed, the shape of the potential energy curve is not particularly sharp but rather flat. The tunneling correction calculated using an Eckart model is thus only a little larger than unity, thus showing that tunneling corrections are probably not significant for this kind of reaction.

3.3. High-Temperature Pathway: Heterogeneous Growth. The identification of the reaction kinetics active during the ZnSe MOVPE is a task complicated by the contemporary presence of gas-phase and surface processes. Accordingly, the development of a kinetic model that can describe the gas-phase reactivity during the ZnSe MOVPE cannot be performed without considering the presence of active surface chemistry. In fact, as a result of the growth process, several species, in particular, radical hydrocarbons, are often produced at the surface. The molecules so generated can then react in the gas phase with $Zn(CH_3)_2$ and H_2Se, starting reaction pathways that would not otherwise have been expected. For the MOCVD of CdTe from $Cd(CH_3)_2$ and $Te(CH_3)_2$, it is known that methyl radicals are desorbed from the growing surface as a result of $Cd(CH_3)_2$ adsorption.[29] It is also known that during the growth of GaAs, three methyl radicals are produced at the surface as a result of the dissociative adsorption of $Ga(CH_3)_3$.[30,31] The (100) surface of the ZnSe growing film is terminated with the Se reconstructed 2×1 surface, which, with respect to Zn atoms, can give rise to a more stable surface.[32−34] Following the mechanism proposed by Moscatelli et al.,[7] we used the below reported surface mechanism to describe the growth process:

$$Zn(CH_3)_2 + \sigma \leftrightarrow [Zn(CH_3)]_{ads} + CH_3\bullet \quad (19)$$

$$H_2Se + 2\sigma \rightarrow [HSe]_{ads} + [H]_{ads} \quad (20)$$

$$[Zn(CH_3)]_{ads} + [HSe]_{ads} \rightarrow ZnSe_{film} + CH_4 + 2\sigma \quad (21)$$

$$[H]_{ads} \rightarrow \frac{1}{2}H_2 + \sigma \quad (22)$$

The reaction is started by the dissociative adsorption of $Zn(CH_3)_2$ on the 2×1 reconstructed Se surface, which results in the formation of the $ZnCH_3^*$ adsorbed species and in a desorbing methyl radical. Calculation performed at the B3LYP/SDD level have shown that this reaction is exothermic by 14 kcal/mol.[7] $Zn(CH_3)^*_{ads}$ reacts successively with H_2Se and H^*_{ads}, leading to the desorption of CH_4 and H_2 and to the growth of the film by a ZnSe unit. The global reaction mechanism is the following:

$$Zn(CH_3)_2 + H_2Se \xrightarrow{\text{surface}} ZnSe_{film} + CH_4 + CH_3\bullet + \frac{1}{2}H_2 \quad (23)$$

At typical growth temperatures, the deposition is in the kinetically controlled regime. Because in this condition mass transport is faster than chemical reactions, methyl radicals diffuse rapidly in the gas phase. These molecules are highly reactive, and when they come into contact with Zn and Se gas-phase molecules, it is reasonable that they start a radical chain mechanism. To verify this hypothesis, the enthalpy changes for several possible gas-phase reactions were computed at the B3LYP level with the 6-311G(d,p) and SDD basis sets. It was thus possible to identify a large number of exothermic neutral−radical and radical−radical reactions, of which the most significant are reported in Table 6. A reaction path proceeding through successive exothermic reactions that have negligible activation energies and lead to the formation of ZnSe adducts could thus be identified. As $CH_3\bullet$ desorbs from the surface, it is likely to react with H_2, which is present in a large amount as the carrier gas. Alternatively, $CH_3\bullet$ can react with H_2Se and $Zn(CH_3)_2$. The reaction with $Zn(CH_3)_2$ to give C_2H_6 was not considered because these reactions are usually forbidden by a large activation energy.[29] Accordingly, the most likely $CH_3\bullet$ reactions were

$$CH_3\bullet + H_2 \rightarrow CH_4 + H\bullet \quad (24)$$

$$CH_3\bullet + H_2Se \rightarrow HSe\bullet + CH_4 \quad (25)$$

Kinetic constants for reaction 24 (and for all reactions among hydrocarbons) and reaction 25 were taken from the literature.[35] Reaction 24 proceeds quickly because of the large amount of

TABLE 6: Reaction Enthalpy Changes (kcal/mol) Calculated at 298 K and 1 atm with B3LYP and Two Different Basis Sets (6-311G(d,p) and SDD) for Several Reactions Involved in the Radical Chain Mechanism

	reaction	ΔH 6-311G(d,p)	ΔH SDD
rc1	$H\bullet + H_2Se \rightarrow HSe\bullet + H_2$	−24.8	−31.3
rc2	$H\bullet + Zn(CH_3)_2 \rightarrow CH_3Zn\bullet + CH_4$	−37.7	−38.4
rc3	$CH_3Zn\bullet + H_2Se \rightarrow CH_3ZnSeH + H\bullet$	−33.0	−36.5
rc4	$HSe\bullet + Zn(CH_3)_2 \rightarrow CH_3ZnSeH + CH_3\bullet$	−31.9	−34.7
rc5	$Zn(CH_3)_2 + CH_3ZnSe\bullet \rightarrow CH_3ZnSeZnCH_3 + CH_3\bullet$	−9.9	−5.4
rc6	$CH_3\bullet + H_2Se \rightarrow HSe\bullet + CH_4$	−23.3	−29.8
rc7	$CH_3Zn\bullet + HSe\bullet \rightarrow CH_3ZnSeH$	−72.3	−69.6
rc8	$H\bullet + CH_3ZnSeH \rightarrow CH_3ZnSe\bullet + H_2$	−25.0	−31.8
rc9	$HSe\bullet + CH_3ZnSeH \rightarrow HSeZnSe\bullet + CH_4$	−30.0	−32.3
rc10	$H\bullet + CH_3ZnSe\bullet \rightarrow CH_3ZnSeH$	−78.9	−73.0
rc11	$H\bullet + HSeZnSe\bullet \rightarrow HSeZnSeH$	−77.9	−72.5

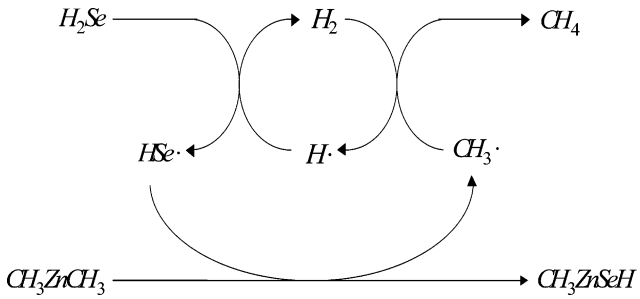

Figure 5. Radical chain mechanism proposed to explain the formation of large gas-phase adducts through reactions started from the CH_3 radicals that desorb from the surface during the growth process.

hydrogen present in the gas phase, thus generating atomic hydrogen that can then react with $(CH_3)_2Zn$ and H_2Se to give $CH_3Zn\bullet$ and $HSe\bullet$ as

$$H\bullet + H_2Se \rightarrow HSe\bullet + H_2 \quad (26)$$

$$H\bullet + (CH_3)_2Zn \rightarrow CH_3Zn\bullet + CH_4 \quad (27)$$

Although reaction 26 is barrierless, the reaction between hydrogen and $Zn(CH_3)_2$ requires an activation energy of 12 kcal/mol, thus too high to proceed at a significant rate in the system considered here. Also, the reaction between $CH_3Zn\bullet$ and H_2Se was found to require a high activation energy of 17.5 kcal/mol, with a preexponential factor of 2.4×10^9 $cm^3/(mol\cdot s)$. Thus, the pathway of adducts formation started by $CH_3Zn\bullet$ radicals, and generally from $R-Zn\bullet$, was considered to be inactive under these conditions. The situation is different for what concerns the reactivity of $HSe\bullet$. In fact, $HSe\bullet$ radicals, produced by reactions 25 and 26, can react with $(CH_3)_2Zn$ to form the first ZnSe adduct, CH_3ZnSeH, and methyl according to the following reaction:

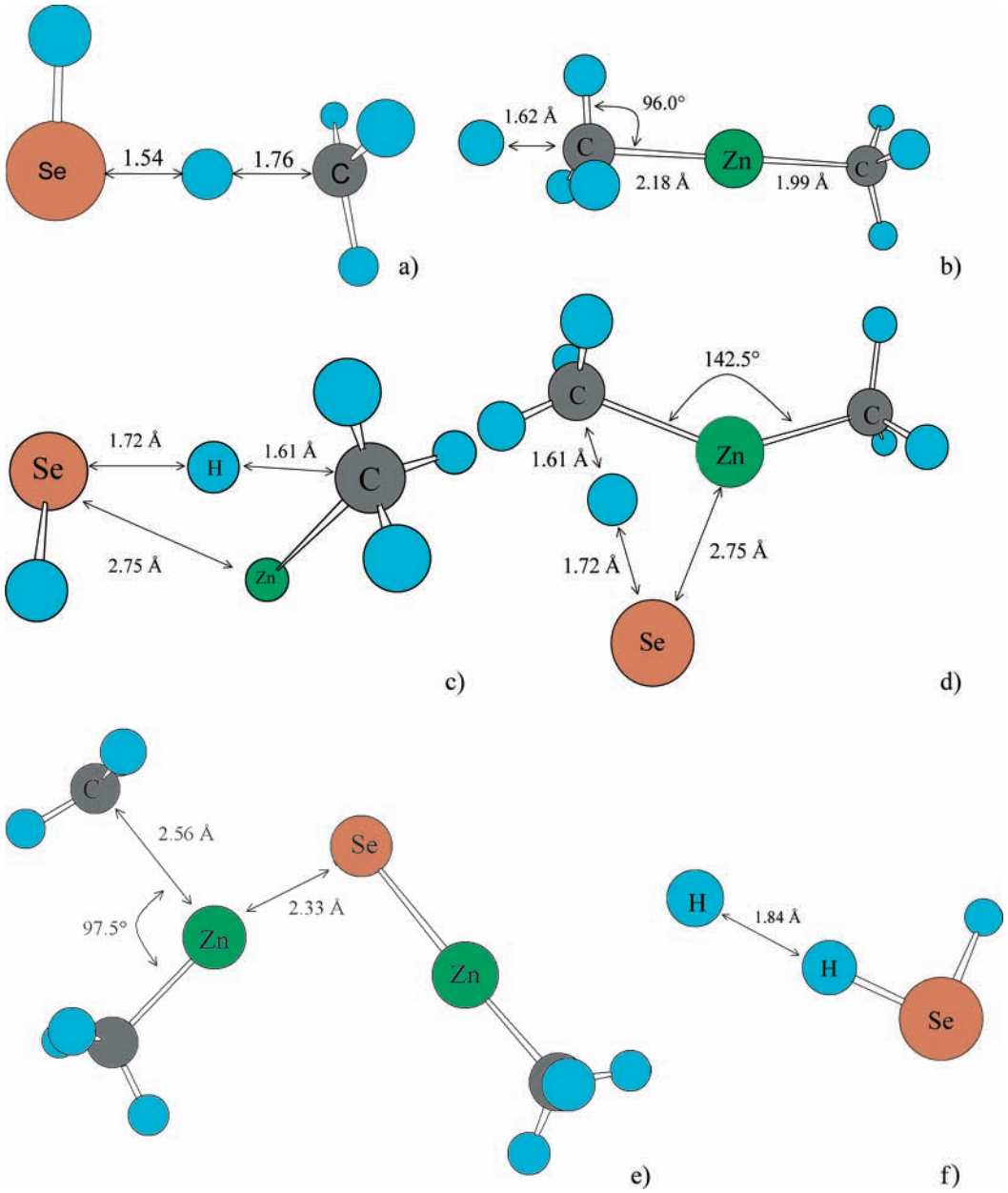

Figure 6. Transition-state structures for several reactions between radicals and ZnSe adducts studied at the B3LYP/6-311G(d,p) level: (a) $CH_3\bullet + H_2Se \rightarrow HSe\bullet + CH_4$, (b) $H\bullet + Zn(CH_3)_2 \rightarrow CH_3Zn\bullet + CH_4$, (c) $CH_3Zn\bullet + H_2Se \rightarrow CH_3ZnSeH + H\bullet$, (d) $HSe\bullet + Zn(CH_3)_2 \rightarrow CH_3ZnSeH + CH_3\bullet$, (e) $Zn(CH_3)_2 + CH_3ZnSe\bullet \rightarrow CH_3ZnSeZnCH_3 + CH_3\bullet$, and (f) $H\bullet + H_2Se \rightarrow HSe\bullet + H_2$.

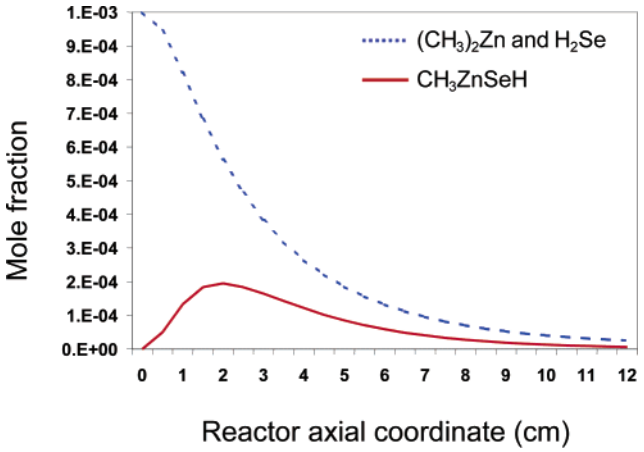

Figure 7. Mole fractions of metal−organic precursors $Zn(CH_3)_2$ and H_2Se and of the first ZnSe gas-phase adduct calculated through a 1D simulation of a typical horizontal ZnSe deposition reactor and reported as a function of the reactor axial coordinate. The simulations were performed using a kinetic scheme comprising the radical chain mechanism of Table 6 and the surface kinetic mechanism reported in the text. Simulations were performed at 260 °C and 250 Torr.

$$HSe\bullet + (CH_3)_2Zn \rightarrow CH_3ZnSeH + CH_3\bullet \qquad (28)$$

The activation energy and preexponential factor for this reaction were calculated to be 2.0×10^{15} $cm^3/(mol \cdot s)$ and 0 kcal/mol. As can be observed, reactions 25 and 28 are almost barrierless, with $CH_3\bullet$ playing the role of a catalyst because it is consumed in reaction 25 and produced again in reaction 28. $CH_3\bullet$ can again react successively with CH_3ZnSeH, extracting H and generating again a reactive ZnSe molecule. This mechanism can lead to the formation of ZnSe gas-phase molecules of large dimensions through a reaction pathway shown in Figure 5. The last steps of the mechanism are recombination reactions:

$$H\bullet/CH_3\bullet + H\bullet/CH_3\bullet \rightarrow H_2/CH_4/C_2H_6 \qquad (29)$$

$$CH_3Zn\bullet + HSe\bullet \rightarrow CH_3ZnSeH \qquad (30)$$

Results obtained with smaller adducts highlighted that the reactivity of R−Se• radicals does not depend on the substituent group R, so the same energetic barrier was considered for similar reactions. Transition-state structures for the basic radical reactions investigated are shown in Figure 6. The largest adduct considered has been $CH_3(ZnSe)_3H$ because after the formation of this adduct cyclization and therefore a change in the reaction mechanism are likely to occur.

The capability of the kinetic mechanism proposed here to explain the formation of gas-phase adducts was tested through the simulation of a typical deposition process.

The simulation was performed at 250 Torr and 260 °C, which are typical operating conditions for the deposition of ZnSe. The mole fractions of the reactants and of CH_3ZnSeH, calculated as a function of the axial coordinate, are reported in Figure 7. If the radical chain mechanism is not inserted into the reactor model, then the mole fraction of CH_3ZnSeH formed would drop to 10^{-9}. It is possible to observe that under these conditions the formation of CH_3ZnSeH is determined mainly by the radical chain mechanism. In Figure 7, it is also possible to observe that after being produced in the first part of the reactor CH_3-ZnSeH further reacts to form larger ZnSe gas-phase adducts. Finally, several simulations were performed to investigate the effect of operating conditions on the formation of large ZnSe

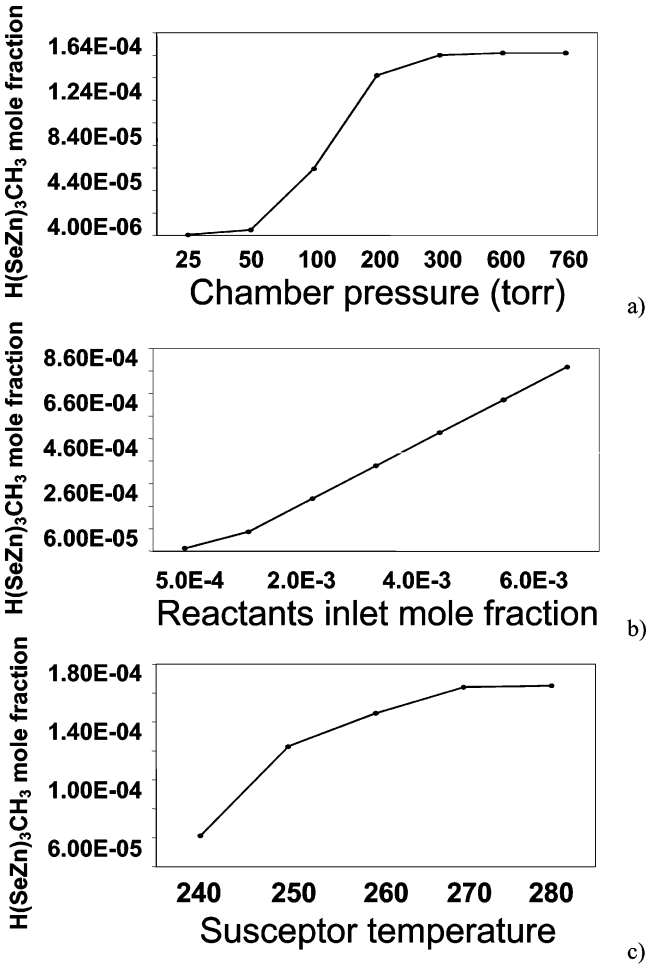

Figure 8. Calculated mole fraction of $H(SeZn)_3CH_3$ produced as a function of (a) chamber pressure (Torr), (b) reactants inlet mole fraction, and (c) susceptor temperature (°C).

adducts. In Figure 8a, we report the mole fraction of CH_3-$(ZnSe)_3H$ produced as a function of chamber pressure, which shows that the formation of adducts is influenced by the pressure at which the reactor is operated. Then, as expected, it was found that the formation of adducts is proportional to the inlet reactants mole fraction (Figure 8b). Finally, the mole fraction of CH_3-$(ZnSe)_3H$ produced as a function of temperature was examined. The results reported in Figure 8c show that an increase in temperature corresponds to only a slight increase in the adduct formation rate.

Summary and Conclusions

The deposition of ZnSe from H_2Se and $Zn(CH_3)_2$ has been studied using theoretical methods. Two deposition processes, one working at low and the other at high temperatures, were investigated. On the basis of our calculations, we found that the mechanism usually proposed in the literature to describe the gas-phase reactivity of Zn and Se molecules cannot justify the experimentally observed formation of ZnSe adducts. In particular, the gas-phase nucleation of ZnSe nanoclusters cannot be explained simply in terms of direct reaction between H_2Se and $Zn(CH_3)_2$. Therefore, we propose that two alternative gas-phase mechanisms are possible. The first one is active at low temperatures, at high partial pressures of H_2Se and $Zn(CH_3)_2$, and in the absence of a heated susceptor. It is started by the formation of clusters of H_2Se and $Zn(CH_3)_2$ molecules, which are stable because of the formation of weak van der Waals bonds

of 5−7 kcal/mol and for high entropies determined by several internal motions, such as free torsional rotors or degenerate bends. The reactivity of these clusters is higher than that of the separated molecules because of the stabilization of the transition states due to the donation of electrons from molecules that are part of the cluster but do not take part directly in the reaction. A simulation of the experimental deposition process with the proposed reaction mechanism has shown that it is consistent with the formation of ZnSe nanoclusters observed. At high temperatures (i.e., higher than 200 °C) and in the presence of a heated susceptor, a different mechanism is possible. It consists of a radical chain mechanism started from the desorption of methyl radicals from the growing surface. This mechanism proceeds through the formation of selenium radicals that successively react with $Zn(CH_3)_2$ or a suitable ZnSe adduct to give the formation of a new ZnSe bond and the production of a CH_4 molecule. Also, in this case, the capability of the proposed mechanism to explain the formation of ZnSe adducts was tested through the simulation of an experimental MOVPE reactor.

References and Notes

(1) Jones, A. C.; O'Brien, P. *CVD of Compound Semiconductors*; VHC: Weinheim, Germany, 1997.

(2) Prete, P.; Lovergine, N.; Traversa, M.; Mancini, A. M. *IC MOVPE XI*; Berlin, 2002; p 147.

(3) *Joint Venture to Produce ZnSe-based White LEDs*. In *Compound Semiconductor*; IOP, Ltd.: Bristol, U.K., Jan-Feb 2003; p 5.

(4) Garcia, A.; Northrup, J. E. *J. Vac. Sci. Technol., B* **1994**, *12*, 2678.

(5) Prete, P.; Lovergine, N. *Prog. Cryst. Growth Charact. Mater.* **2002**, *44*, 1.

(6) Hitchmann, M. L.; Jensen, K. F. *Chemical Vapor Deposition: Principles and Applications*; Academic Press: London, 1993.

(7) Moscatelli, D.; Cavallotti, C.; Masi, M.; Carrà, S. *J. Cryst. Growth* **2003**, *248*, 31.

(8) Sargiannis, D.; John, D. P.; Kioseoglou, G.; Petrou, A.; Mountziaris, T. J. *Appl. Phys. Lett.* **2002**, *80*, 4024.

(9) Karanikolos, G. N.; Alexandridis, P.; Mountziaris, T. J. *J. Phys. Chem B*, submitted for publication, 2003.

(10) Becke, A. D. *J. Chem. Phys.* **1993**, *98*, 5648.

(11) Lee, C.; Yang, W.; Parr, R. G. *Phys. Rev. B* **1988**, *37*, 785.

(12) Cavallotti, C.; Bertani, V.; Masi, M.; Carra, S. *J. Electrochem. Soc.* **1999**, *146*, 3277.

(13) Cavallotti, C.; Masi, M.; Lovergine, N.; Prete, P.; Mancini, A. M.; Carra, S. *J. Phys. IV* **1999**, *9*, 33.

(14) Masi, M.; Cavallotti, C.; Radaelli, G.; Carra, S. *Cryst. Res. Technol.* **1997**, *32*, 1125.

(15) Dunning, T. H., Jr.; Hay, P. J. *Methods of Electronic Structure Theory*; Schaefer, H. F., III, Ed.; Modern Theoretical Chemistry; Plenum Press: New York, 1977; Vol. 3, p 1.

(16) Fuentealba, P.; Preuss, H.; Stoll, H.; Szentpaly, L. V. *Chem. Phys. Lett.* **1989**, *89*, 418.

(17) Hohenberg, P.; Kohn, W. *Phys. Rev. B* **1964**, *136*, 864.

(18) Kohn, W.; Sham, L. J. *Phys. Rev. A* **1965**, *140*, 1133.

(19) Curtiss, L. A.; Raghavachari, K.; Pople, J. A. *J. Chem. Phys.* **1993**, *98*, 1293.

(20) Frisch, M. J.; Head-Gordon, M.; Pople, J. A. *Chem. Phys. Lett.* **1990**, *166*, 281.

(21) Pople, J. A.; Head-Gordon, M.; Raghavachari, K. *J. Chem. Phys.* **1987**, *87*, 5968.

(22) Peng, C.; Ayala, P. Y.; Schlegel, H. B.; Frisch, M. J. *J. Comput. Chem.* **1996**, *17*, 49.

(23) Frisch, M. J.; Trucks, G. W.; Schlegel, H. B.; Scuseria, G. E.; Robb, M. A.; Cheeseman, J. R.; Zakrzewski, V. G.; Montgomery, J. A., Jr.; Stratmann, R. E.; Burant, J. C.; Dapprich, S.; Millam, J. M.; Daniels, A. D.; Kudin, K. N.; Strain, M. C.; Farkas, O.; Tomasi, J.; Barone, V.; Cossi, M.; Cammi, R.; Mennucci, B.; Pomelli, C.; Adamo, C.; Clifford, S.; Ochterski, J.; Petersson, G. A.; Ayala, P. Y.; Cui, Q.; Morokuma, K.; Malick, D. K.; Rabuck, A. D.; Raghavachari, K.; Foresman, J. B.; Cioslowski, J.; Ortiz, J. V.; Stefanov, B. B.; Liu, G.; Liashenko, A.; Piskorz, P.; Komaromi, I.; Gomperts, R.; Martin, R. L.; Fox, D. J.; Keith, T.; Al-Laham, M. A.; Peng, C. Y.; Nanayakkara, A.; Gonzalez, C.; Challacombe, M.; Gill, P. M. W.; Johnson, B. G.; Chen, W.; Wong, M. W.; Andres, J. L.; Head-Gordon, M.; Replogle, E. S.; Pople, J. A. *Gaussian 98*, revision A.5; Gaussian, Inc.: Pittsburgh, PA, 1998.

(24) Truhlar, D. G.; Garrett, B. C.; Klippenstein, S. J. *J. Phys. Chem.* **1996**, *100*, 12771.

(25) Gilbert, R. G.; Smith, S. C. *Theory of Unimolecular and Recombination Reactions*; Blackwell Scientific Publications: Oxford, England, 1990.

(26) Cavallotti, C.; Gupta, V.; Sieber, C.; Jensen, K. F. *Phys. Chem. Chem. Phys.* **2003**, *5*, 2818.

(27) Jensen, K. F.; Pragada, A. A.; Ho, K. L.; Hug, J. S.; Patrick, S.; Salim, S. *J. Phys., Colloq.* **1991**, *4*, C2.

(28) Truong, T. N.; Duncan, W. T.; Tirtowidjojo, M. *Phys. Chem. Chem. Phys.* **1999**, *1*, 1061.

(29) Cavallotti, C.; Bertani, V.; Masi, M.; Carrà, S. *J. Electrochem. Soc.* **1999**, *146*, 3277.

(30) Goringe, C. M.; Clark, L. J.; Lee, M. H.; Payne, M. C.; Stich, I.; White, J. A.; Gillan, M. J.; Sutton, A. P. *J. Phys. Chem. B* **1997**, *101*, 1498.

(31) Cavallotti, C.; Nemirovskaya, M.; Jensen, K. F. *J. Cryst. Growth* **2003**, *248*, 411.

(32) Chen, W.; Kahn, A. *Phys. Rev. B* **1994**, *49*, 10790.

(33) Park, C. H.; Chadi, D. J. *Phys. Rev. B* **1994**, *49*, 16467.

(34) Tomiya, S.; Minatoya, H.; Tsukamoto, H.; Itoh, S.; Nakano, K.; Morita, E.; Ishibashi, A. *J. Appl. Phys.* **1997**, *82*, 2938.

(35) *CRC Handbook of Chemistry and Physics*; Weast, R. C., Ed.; CRC Press: Boca Raton, FL, 1988.

(36) De Maria, G.; Goldfinger, P.; Malaspina, L.; Piacente, V. *Trans. Faraday Soc.* **1965**, *61*, 2146.